European Journal of Pharmaceutical Sciences 207 (2025) 107039

Contents lists available at ScienceDirect

European Journal of Pharmaceutical Sciences

journal homepage: www.elsevier.com/locate/ejps

# $A_{2A}$ receptor antagonist 4-(2-((6-Amino-9-ethyl-8-(furan-2-yl)-9H-purin-2-yl)amino)ethyl)phenol, a promising adenosine derivative for glioblastoma treatment

Akshaya Murugesan [a,b,c,1], Aleksei Smirnov [d,1], Anxo Vila Alonso [a,b], Michela Buccioni [d], Chang Cui [d], Diego Dal Ben [d], Beatrice Francucci [d], Catia Lambertucci [d], Gabriella Marucci [d], Rosaria Volpini [d], Saravanan Konda Mani [e], Sandhanasamy Devanesan [f], Mohamad S. AlSalhi [f], Olli Yli-Harja [g], Andrea Spinaci [b,*], Meenakshisundaram Kandhavelu [a,b,*]

[a] Molecular Signaling Group, Faculty of Medicine and Health Technology, Tampere University, Tampere, Finland
[b] BioMeditech and Tays Cancer Center, Tampere University, Hospital, P.O. Box 553, 33101 Tampere, Finland
[c] Department of Biotechnology, Lady Doak College, Thallakulam, Madurai, India
[d] Medicinal Chemistry Unit, School of Pharmacy, University of Camerino, 62032 Camerino, Italy
[e] B-Aatral Biosciences Private Limited, Bangalore 560091, Karnataka, India
[f] Department of Physics and Astronomy, College of Science, King Saud University, P. O. Box 2455, Riyadh 11451, Saudi Arabia
[g] Computaional Systems Biology Group, Faculty of Medicine and Health Technology, Tampere University, Tampere, Finland

ARTICLE INFO

*Keywords:*
Adenosine analogs
$A_{2A}$AR antagonist
ANR 672
Glioblastoma
Cell death
3D spheroids
Blood brain barrier

ABSTRACT

Adenosine, a pervasive signaling molecule mediated by its interaction with G-protein-coupled receptor subtypes, especially the $A_{2A}$ adenosine receptor ($A_{2A}$AR), plays a crucial role in cancer treatment. Recently, $A_{2A}$AR targeting adenosine analogs have been proposed as a potential therapeutic target for cancer treatment. However, the molecules targeting $A_{2A}$AR and their mode of action in inhibiting glioblastoma cell progression remain unknown. We synthesized six adenosine derivatives substituted at the 9-, 2- and/or $N^{6-}$ and/or 8- positions, and their anti-proliferative efficacy against the GBM cell lines LN229 and SNB19 was assessed. Molecular dynamic simulation integrated with experimental analyses, including cell cycle arrest, apoptosis assay, ligand binding assay, absorption, distribution, metabolism, excretion and toxicity (ADMET) profiling, PAMPA assay, and 3D spheroid analysis, were performed to identify the interaction efficacy of the potential derivative with $A_{2A}$AR and its ability to prevent GBM cell progression. The most potent $A_{2A}$AR derivative (ANR), 4-(2-((6-Amino-9-ethyl-8-(furan-2-yl)-9H-purin-2-yl)amino)ethyl)phenol (ANR 672) inhibits 5′-N-Ethylcarboxamidoadenosine (**NECA**)-induced cAMP validating the antagonistic property with higher cytotoxicity effect against GBM cells. ANR 672 showed higher affinity toward $A_{2A}$AR ($K_i = 1.02 \pm 0.06$ nM) and exhibited significant $IC_{50}$ concentrations of ~ 60–80 μM, than FDA approved drug istredefylline. The $A_{2A}$AR-ANR 672 interaction profile showed well-defined hydrogen bonds and hydrophobic contacts, indicating a typical binding mechanism inside the receptor pocket and a higher degree of conformational flexibility than the $A_{2A}$AR-Istradefylline complex. The antagonist effect of ANR 672 blocked the $A_{2A}$AR signaling pathway, leading to necrosis-mediated cell death and cell cycle arrest at the S-phase in both the GBM cells. ANR 672 treated 3D tumour spheroids analysis with real-time spheroid volume and cell proliferation analysis revealed the potential ability of ANR 672 against GBM cell growth. Drug-likeness assessments also showed favorable pharmacokinetic profiles for ANR 672. Further validation of blood-brain barrier crossing potential revealed that ANR 672 possesses moderate permeability. Our findings shed light on how ANR 672 exerts its GBM-suppressive effect through the interaction of $A_{2A}$AR. These preclinical results suggest that $A_{2A}$AR blockade could be a unique strategy for treating GBM.

* Corresponding authors.
*E-mail addresses:* andrea.spinaci@unicam.it (A. Spinaci), meenakshisundaram.kandhavelu@tuni.fi (M. Kandhavelu).
[1] Equally contributed.

https://doi.org/10.1016/j.ejps.2025.107039
Received 28 December 2024; Received in revised form 6 February 2025; Accepted 9 February 2025
Available online 10 February 2025

## 1. Introduction

Glioblastoma (GBM) is a debilitating brain tumor, classified as a grade IV astrocytoma with abysmal prognosis (Mutharasu et al., 2022; Tamimi and Juweid, 2017). Hypoxia, reduced oxygen pressure in the GBM environment, influences various types of cell signaling molecules determining the inter and intracellular communications (Erices et al., 2023). Extracellular adenosine has been implicated as a key signaling molecule in adenosine signaling events via the interaction of its individual receptor subtypes, including $A_1$, $A_{2A}$, $A_{2B}$, and $A_3$ (Bova et al., 2022; Marucci et al., 2018). Hypoxic circumstances in high-grade glioma (GBM) and low-grade gliomas (LGG) cause HIF-1α to upregulate CD39 and CD73, leading to increased adenosine levels in the tumor microenvironment, promoting disease progression (Domènech et al., 2021). Specifically, accumulation of adenosine affects the downstream signaling pathway of the $A_{2A}$ adenosine receptor ($A_{2A}$AR) signaling pathway, thus activating and inducing Rap1 and PIP3, respectively, ultimately activating the PIK3/AKT signal, driving tumor cell growth and metastasis (Ma et al., 2019). In addition, adenosine, as a tumor-protective target, protects GBM cells and inhibits the efficacy of the existing chemotherapeutic agent, temozolomide. Co-administration of FDA-approved $A_{2A}$AR agonists, regadenoson with temozolomide improved 60 % transport of temozolomide across the blood-brain barrier without affecting the plasma concentration (Jackson et al., 2016). Evidence from The Cancer Genome Atlas (TCGA) database of glioblastoma, thyroid carcinoma, and uveal melanoma unveils the significant role of adenosine signaling in progression-free survival (Sidders et al., 2020).

$A_{2A}$AR, a G-protein-coupled receptor, is a biomarker for many cancers including GBM (Xia et al., 2023). Deletion of $A_{2A}$AR inhibits proliferation and cell cycle resulting in better anti-tumor response, demonstrating its crucial role in GBM disease pathology and treatment (Jin et al., 2021). Despite the use of selective and non-selective agonists of $A_{2A}$AR, the development of adenosine receptor antagonists represents a better alternative treatment for GBM. Other than GBM, $A_{2A}$AR antagonists were found to be effective against many types of tumors, including prostate, renal, colon, head, and neck cancers. Istradefylline, an FDA-approved drug, shows a higher affinity for $A_{2A}$AR than $A_1$AR and has been used to treat Parkinson's disease (Mohan et al., 2021). It is proven to reduce migration, adhesion, and colony formation in B16F10 melanoma cells. Among other small molecules, AB928, AB680, BAY-545, CPI-444, AZD4635, preladenant, SCH-442,416, SCH58261, ZM241385 have emerged as $A_{2A}$AR antagonists with clinical potential (Leone and Emens, 2018; Mohan et al., 2021).

Previously, we have designed and synthesized several adenine derivatives bearing 8-substituted 9-ethyladenines (ANR) with $A_{2A}$AR antagonist potential. Additionally, two series of compounds based on purine and triazolotriazine scaffolds were synthesized and identified as potential $A_{2A}$AR antagonists (Camaioni et al., 1998; Spinaci et al., 2023, 2022). Out of all synthesized ANR derivatives, ANR 672 exerts potential anti-inflammatory properties in a microglial model of neuroinflammation. However, the efficacy of these small molecule $A_{2A}$AR antagonists in treating GBM is yet to be investigated. The present work is addressed to evaluate the effect of selective $A_{2A}$AR antagonists against GBM cells, thus anticipating repurposing and correlating the pharmacodynamic behaviour of the potential antagonists for GBM treatment.

A few of the designed ANR antagonists were synthesized, including ANR 681, ANR 672, ANR 668, ANR 665, ANR 474, and ANR 94, for further investigation. Docking and molecular simulations were performed to investigate the ligand interactions with $A_{2A}$AR receptor. The effect of those ANR antagonists in regulating the $A_{2A}$AR down/stream signaling pathway was identified in 2D and 3D GBM environments (Klowss et al., n.d.). The top potential antagonist against the growth of GBM was also explored through several *in vitro* experiments, including dose-responsiveness, apoptosis, and cell cycle analysis. 3D tumor spheroid experiment was also studied to identify the efficacy of potential ANR antagonists in the GMB cell progression. Additionally, ADMET analysis along with the experimental *in vitro* validation of the lead antagonist to cross the blood–brain barrier (BBB) was also performed.

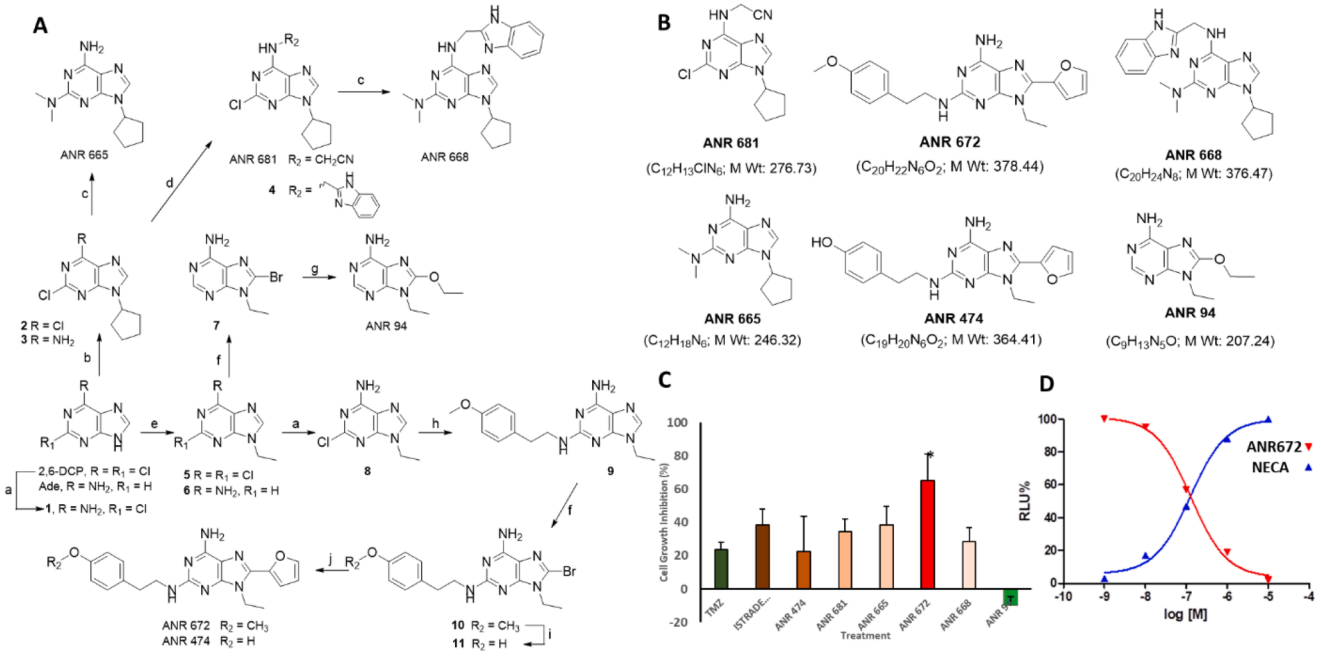


**Fig. 1.** **(A)** Synthesis scheme of the adenine derivatives (ANR). Reagents and conditions: a. $NH_3$ l, r.t.; 16 h; b. Cyclopentyl bromide, dry $K_2CO_3$, dry DMF, r.t., 5 days; c. $NH(CH_3)_2$, 100 °C, 12 h; d. $NH_2CH_2CN$, $Et_3N$, THF, r.t. 18 h; or 2-aminomethyl-benzimidazole, $Et_3N$, DMF, r.t., 30 h; e. EtI, dry $K_2CO_3$, dry DMF, r.t., 16 h; f. N-bromosuccinimide, dry DMF, r.t., 30 min; g. EtOH, NaOH, 100 °C, 24 h; h. 4-methoxy-phenethylamine, 130 °C, 24 h; i. HBr 48 % at 100 °C for 2 h; i. 2 tributylstannyl-furan, $[(Ph)_3P]_2PdCl_2$, dry THF, reflux, 4 h. **(B)** Structure of tested ANRs. **(C)** Cell growth inhibition (%) for the six ANR derivatives, TMZ (drug control) and Istradefylline (positive control) at 100 uM in SNB19 cells. DMSO served as a negative control. All data is represented as mean ± standard deviation (n = 5). * Represent statistically significant differences between the ANR 672 and Istradefylline. * $p > 0,05$, ** $< 0,001$ and ns $p > 0,05$. **(D)** Measurement of cAMP level in human $A_{2A}$AR stably transfected CHO cells treated with ANR 672 and NECA (known $A_{2A}$AR agonist). DCP = dichloropurine, Ade = adenine.

Our findings suggest that the identified $A_{2A}$AR antagonist could competitively inhibit $A_{2A}$AR receptor, thus making them as a potential candidate for GBM therapy.

## 2. Experimental section materials and methods

### 2.1. Chemistry materials

The synthesis scheme for the series of adenine derivatives including, 2-((2-chloro-9-cyclopentyl-9*H*-purin-6-yl)amino)acetonitrile (ANR 681), 4-(2-((6-amino-9-ethyl-8-(furan-2-yl)-9*H*-purin-2-yl)amino)ethyl) phenol (ANR 672), $N^6$-((1*H*-benzo[*d*]imidazol-2-yl)methyl)-9-cyclopentyl-$N^2$,$N^2$-dimethyl-9*H*-purine-2,6-diamine (ANR 668), 9-cyclopentyl-$N^2$,$N^2$-dimethyl-9*H*-purine-2,6-diamine (ANR 665), 9-ethyl-8-(furan-2-yl)-$N^2$-(4-methoxyphenethyl)-9*H*-purine-2,6-diamine (ANR 474), 8-ethoxy-9-ethyl-9*H*-purin-6-amine (ANR 94), is mentioned below.

### 2.2. Synthesis of adenine derivatives

All the synthesized $A_{2A}$AR antagonists are adenine derivatives substituted at the 9-, 2- and/or $N^6$- and/or 8-positions and synthesized from commercially available 2,6-dichloropurine (ANR 681, ANR 672, ANR 668, ANR 665, and ANR 474) (Spinaci et al., 2023, 2022) or adenine (ANR 94) (Fig. 1)(Camaioni et al., 1998; Marucci et al., 2008; Pinna et al., 2005). The first reaction to obtain these derivatives was, generally, the alkylation at the 9-position of the corresponding starting materials by reacting with the suitable alkyl or cycloalkyl halides. Hence, the obtained intermediates were treated with the appropriate amines to have the substitution at the 6- and then at the 2-position. The substituents at the 8-position were introduced after bromination with *N*-bromosuccinimide and then replacement of the 8-bromine atom with ethanol (ANR 94) or tributylstannylfurane (ANR 672 and ANR 474).

### 2.3. Molecular modeling

#### 2.3.1. $A_{2A}$ receptor structure refinement and docking

The crystal structure of human $A_{2A}$AR binding with ZM241385 was obtained from the Protein Data Bank (3EML) with a resolution of 2.6 Å (Doré et al., 2011). The structure of istradefylline was derived from the DrugBank database (Wishart et al., 2006) and serves as a control. ANRs were drawn using the Jmarvin program and saved in the structure-data format (SDF) format. The ligand and the receptor target were saved as separate files for docking purposes. The atoms from the inflexible root were selected to get the rigid root. The rotatable bonds were also employed. The "write pdbq" function was used to save the generated pdbq format, which includes the load parameter for the ligand. AutoDock Vina software is used for virtual screening, which precisely evaluates the binding affinity of small molecules with macromolecular targets (Eberhardt et al., 2021). The software uses an iterative search technique that combines genetic algorithms and local search approaches to examine the ligand's conformational space and interactions with the target. Docking was initiated using AutoDock Vina, and the target macromolecule was introduced with polar hydrogens, and suitable charges were further assigned. The binding site of the target $A_{2A}$AR is determined by defining a grid box that includes the area of interest. The docking parameters, including exhaustiveness, number of modes, and energy range, were then adjusted to achieve a balance between computing efficiency and accuracy. Upon docking, many binding postures were produced that were prioritized based on their estimated binding affinities. The binding interactions and ligand's efficacy in binding with the receptor were visually inspected using the Discovery Studio visualizer.

#### 2.3.2. Molecular dynamic simulation

We have adapted the Amber 18 program (Case et al., 2005) to reveal the binding mode and relative binding efficiency of $A_{2A}$AR with ANR 672 ligand. The protein was disintegrated using a box of rectangular shape with edges at least 10 Å apart using the TIP4PEW water-based model (Izadi et al., 2014). The system was neutralized by introducing the required amount of counter ions (0.15M KCl) using the Monte Carlo ion placing method (Krog et al., 2023). The width of the water layer around the lipid membrane was maintained around 17.5 Å. The parameters were optimized with constant pressure at 1 atm and temperature at 300 K (NPT) to generate the required molecular trajectories. The particle mesh Ewald technique (Darden et al., 1993) was used to effectively deal with long-range electrostatic interactions. The system has been minimized and then equilibrated for a time period of 100 ps and 1 ns, respectively. In addition, the distance cut-off for non-bonded interaction was set to 9 Å. SHAKE algorithm (Barth et al., 1995) was used to limit the vibration of the hydrogen atoms. Molecular production dynamics were analyzed for a period of 100 ns using an NPT ensemble and a 1 fs time step simulation. Finally, the MD trajectories were analyzed to find the root-mean-square deviation (RMSD) and root-mean-square fluctuation (RMSF) to obtain the coordinates.

### 2.4. Biological measurements

#### 2.4.1. Biology materials

Dulbecco's Modified Eagle Medium (DMEM) (Cat. No. D5796–500ML, Sigma-Aldrich, St. Louis, MO, United States), 10 % of fetal bovine serum (FBS) (Cat. No. S181H, Biowest, Nuaillé, France) 0.1 mg/mL Streptomycin and 100 U/mL Penicillin (Cat. No. P4333–100ML, Sigma-Aldrich, St. Louis, MO, United States), TMZ, DMSO, TMZ (chemotherapeutic agent for GBM), Istradefylline (known antagonist for $A_{2A}$AR targeting ligand), propidium iodide (PI) (ThermoFisher Scientific, Waltham, MA, USA), Annexin V-Alexa Fluor™ 488 and PI (REF V13245, ThermoFisher Scientific, Waltham, MA, USA), PBS ((Sigma-Aldrich, St. Louis, MO, USA), BBB-kit (PMBBB-096, BioAssay Systems)

#### 2.4.2. Cell culture analysis

The Chinese hamster ovary cells (CHO) stably transfected with $A_{2A}$AR (generous gift from Prof. Karl-Norbert Klotz, University of Wuerzburg, Germany) was grown in Dulbecco's Modified Eagle Medium (DMEM)/F12 containing 10 % FBS (fetal bovine serum), 100 U/mL penicillin, 100 µg/mL streptomycin, 2.5 µg/mL amphotericin B, 1 mM sodium pyruvate, 0.1 mg/mL Geneticin (G418). The human glioblastoma cell lines LN229, SNB19 (gifted by Prof. Maria Stella Carro, University Medical Center Freiburg, Germany), 1321N1 (Istituto Zooprofilattico, Brescia, Italy), mouse embryonal fibroblast (MEF) (gifted by Prof. Pasi Kallio, Tampere University, Finland) were grown and maintained in DMEM containing 10 % of FBS, 01 % Penicillin-Streptomycin (Product #P4333, Sigma-Aldrich, St. Louis, MO) and 0.025 mg/ml Amphotericin B (Sigma-Aldrich, St. Louis, MO), under standard cell culture conditions (37 °C, 5 % $CO_2$, and 95 % humidity).

#### 2.4.3. High-throughput measurement of cAMP level

The functional activity of compound ANR 672 was assessed using the GloSensor cAMP quantification assay (Promega corporation, Madison, WI) by monitoring the changes in intracellular cAMP. CHO cells, stably expressing the human $A_{2A}$AR and the biosensor, were cultured as described in the manufacturer's protocol. The biosensor encodes a genetically modified form of firefly luciferase into which a cAMP-binding protein moiety has been inserted. The production of cAMP upon receptor stimulation, further binds to the biosensor, and induces a conformational modification leading to light emission. CHO cells at $1.0 \times 10^5$ cells/ml were cultured in growth medium containing DMEM/F12 medium and 10 % FBS.

After 2 h of incubation with the GloSensor cAMP reagent stock solution, cells were seeded into 384-well plate and the reference agonist NECA was added at a fixed concentration of 1 µM. Subsequently ANR 672 was added at various concentrations (10 nM - 10 µM). The

antagonist profile was evaluated by measuring the ability to counteract an increase in cAMP accumulation induced by NECA. Responses were expressed as a percentage of the maximal relative luminescence units (RLU).

Concentration–response curves were fitted by a nonlinear regression using Prism software (GraphPad Software, San Diego, CA, USA). The antagonist profile of the compound was expressed as the $IC_{50}$, which is the concentration of antagonist that produces a 50 % inhibition of the agonist effect.

#### 2.4.4. Cell counting assay

Cytotoxicity assay was performed to assess the growth inhibition of six $A_{2A}$AR antagonists. Initially, the ANR derivatives were tested for its cytotoxicity against GBM cell line, SNB19 cells, at 100 μM concentration. TMZ and Istradefylline were used as a positive and ligand-control respectively, whereas 0.1 % DMSO was used as a negative control. A total of $1 \times 10^5$ cells/well were seeded in 6-well culture plates. After incubation at 37 °C in a humidified atmosphere with 5 % $CO_2$ at 60 −70 % confluence, $A_{2A}$AR antagonists at 100 μM concentration were added separately to each wells containing SNB19 cells. The cells were further incubated for 48 h at cell culture conditions, and then the cells were collected after trypsinization and centrifuged at 800 g for 5 mins. Number of live and dead cells were determined after trypan blue staining using Countess II FL Automated Cell Counter (Thermo Fisher Scientific, Carlsbad, CA, USA) using the Eq. (1)(Karjalainen et al., 2017).

$$Inhibition\,(\%) = \frac{Mean\ of\ untreated\ cells\ (DMSO\ control) - Mean\ of\ treated\ cells}{Mean\ of\ untreated\ cells\ (DMSO\ control)} x100 \quad (1)$$

#### 2.4.5. Inhibitory kinetic assay

Concentration dependent effect of the top antagonist, ANR 672, against the growth of multiple GBM cell lines including LN229 and SNB19 cells was determined using the live and cell death assay described above. The cells were individually seeded in 12 well plate at a density of $3 \times 10^5$ cells/well and incubated at 37 °C for 24 h. At 60–80 % confluence, the cells were treated with varying concentration of ANR 672 including 10 μM, 25 μM, 50 μM, 100 μM and 150 μM and incubated for 48 h in cell culture condition. 0.1 % DMSO was used as negative control, and istradefylline as a positive ligand control. Trypan blue staining was done to identify the percentage of cell growth inhibition using the above-mentioned procedure following the Eq. (1). The dose-response curve was plotted using the percentage of inhibition at each concentration and the half maximal inhibitory concentration ($IC_{50}$) was calculated specific for each cell line. Further, ANR 672 was evaluated on non-cancerous MEF cells to see if it affected the normal cell lines at 150 μM, as the percentage of growth inhibition was higher at this concentration.

#### 2.4.6. Cell cycle analysis by flow cytometry

LN229 and SNB19 cells at 60–80 % confluence was treated with the 100 μM of ANR 672 in 12 well cell culture plate at a density of $3 \times 10^5$ cells/well. 0.1 % of DMSO was used as a negative control. After 48 h of incubation, the cells were resuspended in ice-cold PBS, fixed with 70 % ice-cold ethanol. The cells were then stained with solution containing 1 mL of PI (20 mg/mL), 2 mL of Triton X-100 (1 %) and 100 μL of RNAse (10 mg/mL) for 10 mins at room temperature. The cells were analyzed for PI fluorescence using a flow cytometer (CUBE 8, SYSMEX, Kobe, Japan) at an excitation laser at ~535 nm. The cells were analyzed using FlowJo (v. 10.8.1) and the percentage of cells indicating different phases of cell cycle were estimated by gating the cells using width and area parameters.

#### 2.4.7. Apoptotic assay

LN229 and SNB19 cells were used for the apoptosis assay (Kari et al., 2022) using a Dead cell apoptosis kit with Annexin V-Alexa Fluor™ 488 and PI, following manufacturer's instructions. Cells were seeded in 12 well plate at a density of $3 \times 10^5$ cells/well and maintained in cell culture environment until it reaches the confluence of 60–70 %. The cells were then treated with 100 μM ANR 672 and incubated for 48 h in appropriate humidified atmosphere. The cells were then washed in PBS, collected after centrifugation 450 g for 5 mins at 4 °C and resuspended in 100 μl 1X Annexin-V. The cell suspension containing 400 μL cells with the density of $1 \times 10^5$ cells/mL, 20 μL of Alexa Fluor™ 488 Annexin V and 4 μL PI (100 μg/mL) was prepared and incubated at temperature for 15 mins, with further addition of 400 μL of Annexin-V (1X) to complete the staining process. The cells were analyzed immediately after staining using flow cytometry (CUBE 8, SYSMEX, Kobe, Japan) at an excitation and emission wavelength of 488 nm/530 nm. The data was analyzed using FlowJo (v. 10.8.1) to determine the % of cells in different phases of apoptosis.

#### 2.4.8. Spheroids cell proliferation assay

The GBM cells, 1321N1 and their spheroids (see description in "Cell culture 3D environment" section) were seeded into 96-well cell culture plates at the density of $1 \times 10^4$ in 98 μl od media and incubated overnight. After 24 h, 2 μL of compound were added to the wells. Subsequently, 20 μl of CellTiter reagent were added to the cells and after 1 h of incubation at room temperature the absorbance was recorded at 490 nm with a 96-well plate reader. Cell viability was calculated as percentage using the following formula:

$$\text{Cell viability} = \frac{\text{OD mean of treated cells}}{\text{OD mean of control cells}} x100$$

An untreated control and a control with the solvent were run. All experiments were performed in triplicate.

#### 2.4.9. Time-lapse imaging of 3D spheroids

Cell line 1321N1, was used for the formation of spheroids with the cell density of 750 cells/well in cell repellent U bottom 96 well CELLSTAR® plates (Reference No.650970) and grown in DMEM medium in cell culture environment for 6 days. The uniformity of the spheroids was analyzed and the spheroids with the least inter-well variability was chosen for further experimentation. The spheroids were treated with the 25–150 μM concentration of ANR 672 for 24 h under the same monolayer cell culture environment. A part of the plate was analyzed with MTS (The CellTiter 96® AQueous One Solution Cell Proliferation Assay), while the remaining part was left free for six-treatment proliferation study. For MTS assay, spheroids were incubated for 4 h instead of conventional 1 h, like monolayers. The long-term ability to inhibit the proliferation of solid tumors was confirmed by monitoring the spheroid proliferation for ten days after treatment, compared to non-treated samples. Time-lapse microscopic images were taken (Chowdhury et al., 2012) and measured for its uniformity and changes in spheroid volume using the SpheroidSizer – a MATLAB-based, open-source software application (Chen et al., 2014).

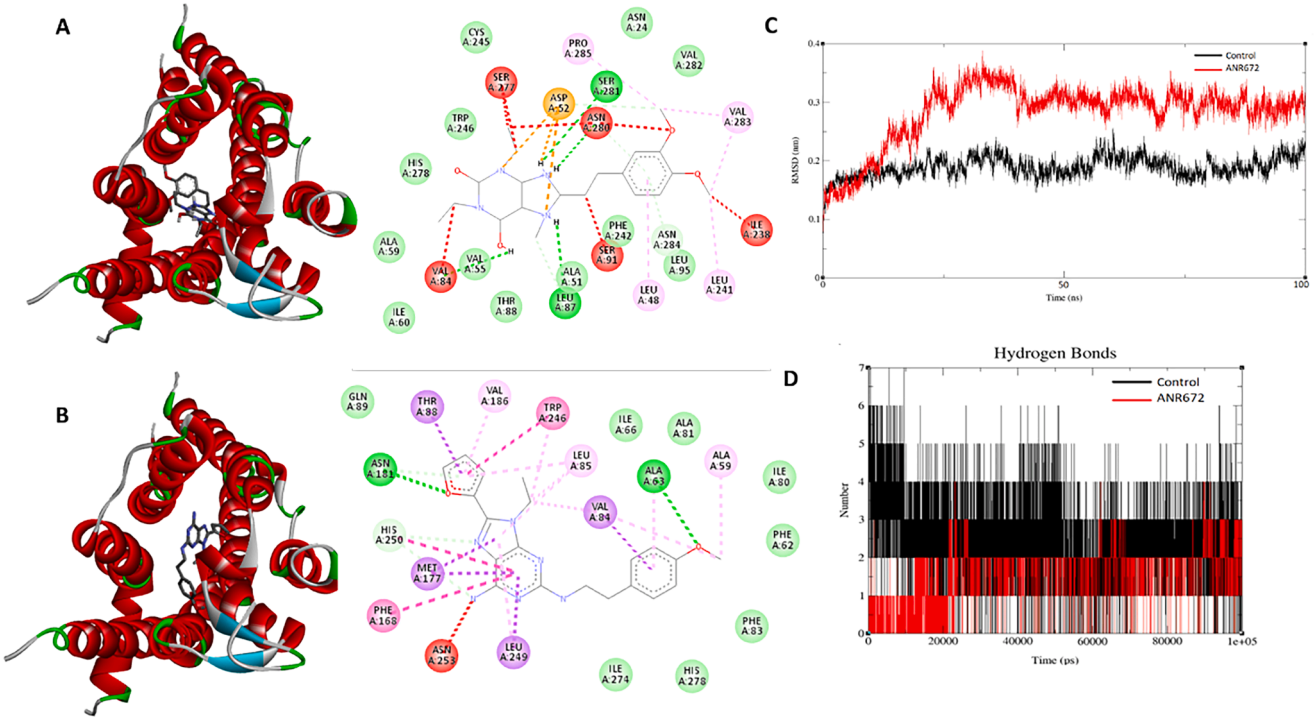


**Fig. 2. Molecular dynamics simulation of ANR 672 derivative and its interaction with target protein.** Representation of the $A_{2A}$AR- Istradefylline (Control) **(A)** and $A_{2A}$AR-ANR 672 **(B).** The protein is shown as a ribbon model with helices in red, loops and grey beta-sheets depicted in cyan. The scaffold of the compound ANR 672 is represented in stick format depicting its binding pocket and residues representing important interactions. Residues forming the interaction are highlighted with labels and colored according to the type of interactions: hydrophobic (green), hydrogen bonds (orange), π-π stacking (blue). **(C)** Root Mean Square Deviation (RMSD) plot of the protein-ligand complex during simulation. Root Mean Square Deviation between complex and initial pose over the time of both the controls (black) and complexes, in presence and/or absence of ANR 672 (red). **(D)** Hydrogen bond analysis for the length of a simulation. The black curve is control and the red one represents system with ANR 672, counts of hydrogen bonds between ligand-protein are normalized by time.

*2.4.10. ADMET profiling*

Drug likeness and the ADMET profile of ANR 672 were analyzed using the web program SwissADME (http://www.swissadme.ch/). The Simplified Molecular Input Line Entry System (SMILES) formats of ANR 672 was originally obtained during the synthesis of the compound. Lipinski's rule of 5 was checked for the drug-likeness of ANR 672 to ensure that if all the properties are within the accepted range. The adsorption feature of the ANR 672 was analysed by characterizing the values of human intestinal absorption (HIA), P-glycoprotein substrate/ inhibitor. The ability to distribute the drug across the blood brain barrier (BBB) was also checked. Metabolism of the ANR 672 was assessed based upon the CYP models for substrate or inhibitor, such as CYP1A2, CYP2C19, CYP2C9, CYP2D6, and CYP3A4. All the above-mentioned analysis were performed using SwissADME".

*2.4.11. Parallel artificial membrane permeability assay (PAMPA)*

The prediction of the ANR 672 crossing BBB was evaluated by a parallel artificial membrane permeability assay-BBB kit (PAMPA-BBB). Here, the donor and acceptor 96-well plates were used that works as passive transcellular permeability compartments. Briefly, the donor plate was impregnated with 5 μL of porcine lipids (20 mg mL–1, in dodecane), and 300 μL of PBS with 5 % DMSO was added to the acceptor 96-well plates. Later, 100 μM of ANR 672 dissolved in 200 μL of PBS with 5 % DMSO was immediately added to the donor well and the acceptor well was carefully placed onto the donor well. The permeability system was left undisturbed in humidified pockets to prevent solvent evaporation at the physiological thermodynamic condition at 37 °C for 18 h. The experiment was performed in duplicates with three inter-day repetitions. After incubation period, the donor and acceptor plates were separated and the ANR 672, low permeability control (LPC) and high permeability control (HPC) were quantified at a wavelength of 260nm using Tecan GENios Pro (Switzerland). Compounds were classified as low or high permeable (LP or HP) using a permeability value of 4.0 × 10−6 cm/s as the generalized cutoff (Liew et al., 2015).

*2.4.12. Data and statistical analysis*

All the statistical data were reported as Mean ± SEM. Statistical analyses were carried out using Statistical Package for the Social Science (SPSS). Comparison between two groups of variables was performed by ANOVA with Dunnett's test. All the in-vitro experiments were performed in replicates with n = 6. P values less than 0.05 and 0.001 were considered as statistically significant and indicated as * and **.

## 3. Results

### *3.1. ANR 672 interacts with $A_{2A}$AR and reduce the cell viability in GBM cells*

ANR compounds ANR 681, ANR 672, ANR 668, ANR 665, ANR 474 and ANR 94 were synthesized as described previously (Fig. 1**A**). Purity of all the synthesized compounds were verified from their melting point and through elemental analysis. All compounds are >95 % pure validated by HPLC analysis (Supplemental file). The compound ANR 672 was re-synthesized from the commercially purchased starting material, 2,6-dichloropurine in five steps with a total yield of 6.3 %. 2,6-dichloropurine was alkylated at 9-position by treating with ethyliodide to give the 2,6-dichloro-9-ethylpurine (Spinaci et al., 2023). Then, the amino group in 6th -position of **1** was introduced by treating with ammonia to obtain the adenine derivative **2**, in which the 2-chlorine atom was replaced by reaction with the 4-methoxyphenylethylamine. The resulting 2-(p-methoxyphenethylamine)-9-ethyladenine (**3**) was brominated at 8-position to obtain the 8-bromo derivative **4**, in which the furyl ring

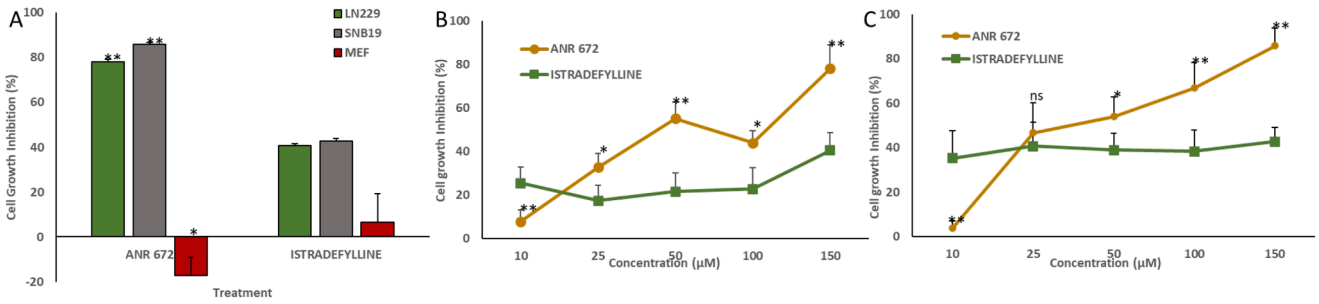


**Fig. 3.** Cell growth inhibition (%) of GBM cells by ANR 672. (A) Inhibition (%) of ANR 672 and Istradefylline in GBM cell lines, LN228, SNB18 and non-cancerous cell, MEF. Cell growth inhibition at varying concentration ANR 672 and Istradefylline (10 uM, 25 uM, 50 uM, 75 uM, 100 uM and 150 uM) in LN229 (B) and SNB19 (C). All data is represented as mean ± standard deviation (n = 5). * denotes statistically significant differences between the ANR 672 and Istradefylline by Dunnett's test; * p > 0,05, ** < 0,001 and ns p > 0,05.

was introduced by the Stille coupling reaction to reach the desired compound ANR 672 (Fig. 1**A**).

The cell growth inhibition assay was performed to study the biological effects of all the six adenosine derivatives (Fig. 1**B**) against the growth of GBM cells, SNB19 cells (Fig. 1**C**). Temozolomide and istradefyline were used as a drug control and positive control, respectively. DMSO was used as a negative control, and the baseline effect was deducted. GBM cell lines were treated with 100 μM concentration of all the six ANR derivatives, TMZ and Istradefylline. Fig. 1**C** shows that, among the tested compounds ANR 672 exhibited the highest cell growth inhibitory effects (65 %), surpassing the current standard drug TMZ (23 %) and istradefylline (38 %). Indeed, 40 % of growth inhibition was recorded for ANR 474, ANR 681, ANR 665 and ANR 668 better than the TMZ and comparable to istradefylline. In contrast, ANR 94 induced the GBM cell growth. This result suggests that ANR 672 had a profound antiproliferative effect on GBM cells than the other derivatives, and hence subsequent analyses were carried out using ANR 672. Further to study on the specificity of $A_{2A}AR$ antagonistic effect in inducing the cell death, cAMP binding assay was performed in $A_{2A}AR$ stably expressed CHO model. It was found that ANR 672 did not enhance cAMP production, indirectly validating the antagonistic effect of ANR 672 when interacting with $A_{2A}AR$. Thus, the antagonist profile was assessed by evaluating its ability to offset an increase in cAMP accumulation triggered by NECA, an agonist of $A_{2A}AR$. The $IC_{50}$ value of ANR 672 in inhibiting cAMP was measured by treating the SNB19 cells with different concentrations of ANR 672 and the dose response curve for ANR 672 and NECA was plotted (Fig. 1**D**). $EC_{50}$ value of ANR 672 and NECA was calculated as 1.305e-007 and 1.253e-007, respectively. These data revealed that ANR 672 exhibited an $IC_{50}$ value of 131 ± 16 nM, suggesting it as an antagonist.

### 3.2. *Mode of interaction of ANR 672 with $A_{2A}AR$ protein*

To obtain further insight into the mechanism of binding of the ANR 672 derivative, a docking investigation was conducted with the human $A_{2A}AR$ protein. The study demonstrated that ANR 672 has a strong affinity for the $A_{2A}AR$ receptor (-10.22 = Kcal/mol). The study also revealed the relative binding energy required to form the ANR 672-$A_{2A}AR$ complex (Fig. 2**A**). The low binding energy of ANR 672 provides an advantage as it implies a strong interaction between the chemical and the receptor binding site. This strong interaction increases the likelihood of inactivating $A_{2A}AR$ activity. The docking investigations have also demonstrated that ANR 672 forms hydrogen bonds with the protein, with all bond lengths measuring less than 3Å, indicating a strong contact. The $A_{2A}AR$-ANR 672 displayed a stable interaction profile with well-defined hydrogen bonds and hydrophobic contacts, indicating a conventional binding mode within the receptor pocket compared to that of the $A_{2A}AR$-Istradefylline complex (Fig. 2**B**).

A molecular dynamics simulation was conducted to investigate the stability and convergence of the $A_{2A}AR$-ANR 672 complex, using the root mean square deviation (RMSD) as the metric for evaluating the outcome. As shown in Fig. 2**C**, the root mean square deviation (RMSD) of the backbone Cα atoms of $A_{2A}AR$ was compared to the starting structure throughout the simulation. Enhanced RMSD in the ANR 672 complex possibly reflects a ligand binding-induced conformational change or flexibility. The results imply that the protein undergoes rapid conformational changes in the early stages but stabilizes after 50 ns and remains stable for the remainder of the simulation.

The picture also illustrates a comparison of the protein structure in apo form and when bound with ANR 672. The 3D structural modeling emphasizes integrating ANR 672 within the binding pocket. The 2D interaction maps reveal distinct variations in the interaction patterns between the control and ANR 672-bound states. Additionally, ANR 672 forms stabilizing interactions with ASN, THR, and PHE residues. These interactions suggest that ANR 672 has the potential to alter the specific circumstances within the binding pocket, consequently impacting the activity of the protein. The higher RMSD values observed for the ANR 672 - bound state indicate that the ligand may have induced conformational changes that could compromise the protein's stability. Fig. 2**D** demonstrates the fluidity of hydrogen bond formation and stability, suggesting that ANR 672 changes not only individual key interactions within the binding site but also affects the conformation of the entire protein. The examination of hydrogen bonds further confirms this observation since it reveals a change in the hydrogen bonding pattern between the ANR 672-bound state and the control, which exhibits a more consistent hydrogen bonding distribution.

These results revealed that the $A_{2A}AR$-ANR 672 complex had a higher degree of conformational flexibility compared to the control, suggesting ligand-induced structural changes. Overall, the findings suggest that the interaction between ANR 672 and the protein significantly impacts the protein's stability, structural flexibility, and potentially its activity.

### 3.3. *In-vitro growth inhibitory effect of ANR 672 on multiple GBM cells, and non-cancerous MEF cell*

The top ANR derivative, ANR 672, was tested for its cytotoxicity effect on SNB19 and LN229 cell proliferation at various concentration (10 μM, 25 μM, 50 μM, 100 μM, and 150 μM). The known $A_{2A}AR$ antagonist, istradefylline, was used as a positive control to comparatively examine the possible inhibitory activity. The results revealed that both ANR 672 selectively suppressed the growth of GBM cells in a dose dependent manner whereas istradefylline doesn't affect the cell growth significantly. Fig. 3**A** demonstrates that ANR 672 inhibits the GBM cell growth at a higher concentration of 150 uM to about 78 % and 86 % for LN229 and SNB19 respectively. Whereas the control drug Istradefylline showed 43 % of inhibition in both the cell lines. Interestingly, ANR 672 demonstrated null and void cytotoxicity in non-cancerous cells, MEF,

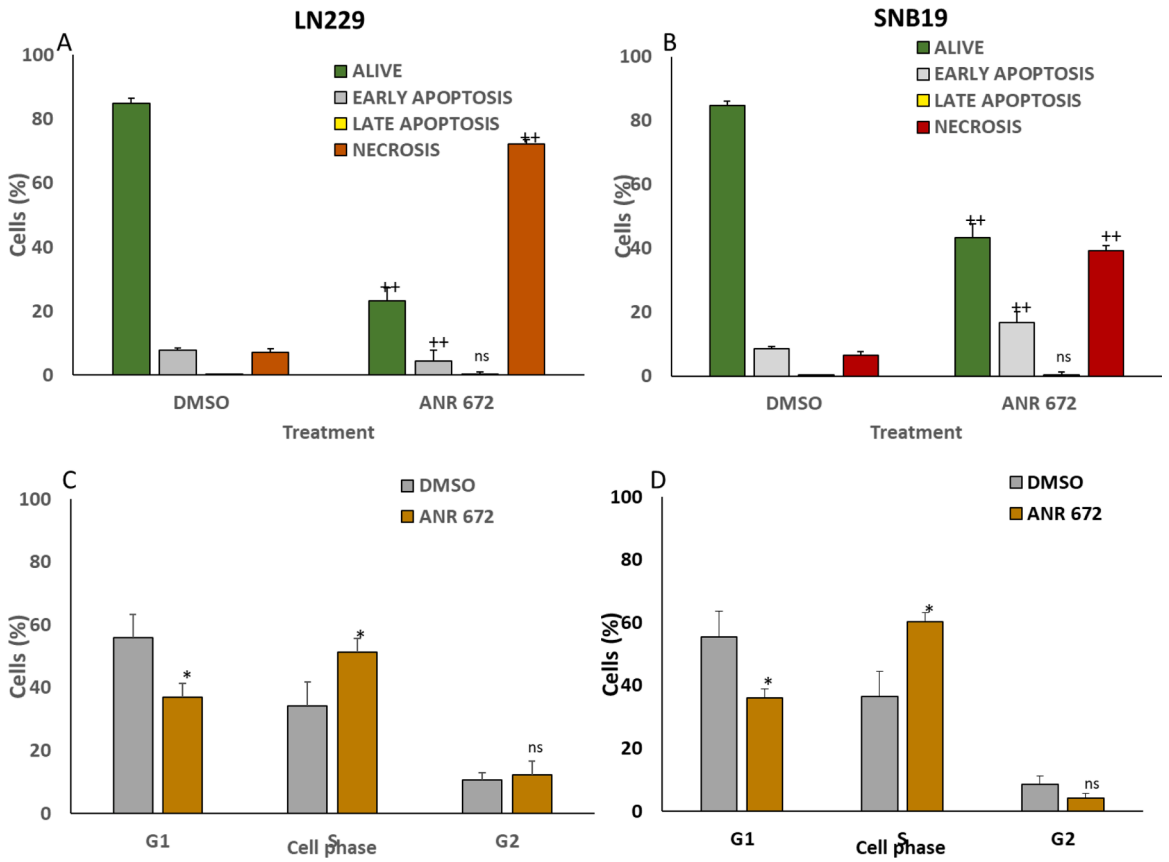


**Fig. 4.** Effect of ANR 672 in inducing apoptosis. Percentage of apoptotic and nectrotic cells in LN229 (A) and in SNB19 cell lines (B) after treatment and ARN 672. (C) Percentage of cells in different phases of cell cycle upon treatment with ANR 672 in LN229 and (D) SNB19 cell lines. DMSO served as a negative control. All the data is represented as mean ± standard deviation (n = 5). * Represent statistically significant differences between the ANR 672 and control by Dunnett's test. * $p > 0,05$, ** $p > 0,001$ and ns $p > 0,05$.

when compared to LN229 and SNB19 cells. At 150 μM, ANR 672 induced MEF cell proliferation by around 20 %, while istradefylline reduced the MEF cell growth to the least level of around 6.5 %. Thus, in both the cell line, ANR 672 showed potential growth inhibition (%) than the Istradefylline, except at 10 μM where it was less effective. In addition, the $IC_{50}$ concentrations for ANR 672 were calculated to be 83.41 μM and 63.98 μM while istredefylline had 374.56 μM and 399.73 μM for LN229 and SNB19, respectively (Fig. 3**B and 3C)**. These findings show that selective binding of ANR 672 could trigger cell death exclusively in GBM cells, but not in MEF cells, which could be owing to ANR 672's interaction with the $A_{2A}$ receptor. Thus, ANR 672 was selected for further investigation to better understand the mechanism of cell growth inhibition in GBM cells.

### *3.4. ANR 672 induces the cycle arrest in the S phase and necrosis in GBM cells*

The ability to induce apoptosis by the ANR 672 as an approach to maintain the balance between cell proliferation and cell death, the apoptosis and necrosis mediated-GBM cell death was determined using flow cytometry using Annexin V-Alexa Fluor™ 488 and PI staining. As shown in Fig. 4**A**, ANR 672 treated LN229 cells has significantly higher percentage of necrotic cells (72 %), compared to DMSO-treated cells (7 %). Similarly, ANR 672 treated SNB19 cells resulted in 56 % cell death, which includes 39 % of necrotic cells and 17 % of apoptotic cells (Fig. 4**B**). The results indicated that ANR 672 might cause a higher percentage of necrosis than apoptosis in both the GBM cells. It was also noticed that the rate of early apoptotic cells was higher than the late apoptotic cells in both LN229 and SNB19 cells, thus suggesting that ANR 672 acts as a DNA damaging agent and promotes necrosis-mediated cell death. However, it is important to elucidate if the reported cytotoxic effect of ANR 672 in GBM cells is due to cell-cycle arrest, we performed PI labeling, followed by flowcytometry. ANR 672 arrested 30 % of both the GBM cells in G1 phase which is significantly lesser than the DMSO treated cells after 48 h of treatment. There was a substantial increase in the percentage of cells in S phase (~68 %) in both LN229 and SNB19 cells (Fig. 4**C and** 4**D**). DMSO treatment resulted in a considerable drop in the percentage of cells S phase, with only 34 % and 39 % in LN229 and SNB19, respectively. Thus, the accumulation of cells in S phase was accompanied by a corresponding decrease in the percentage of cells in G2 phase with only 10 % in DMSO treated and ANR 672 treated LN229 cells. There was no significant difference in the G2 phase of ANR 672 and DMSO treated SNB19 cells (Fig. 4**D**). Overall, our findings demonstrate that ANR 672 can inhibit GBM growth via S phase checkpoint arrest. All the data was processed using FlowJo version 10.8.1.

### *3.5. ANR 672 inhibits GBM spheroid growth*

Long-term spheroid culture was carried out in the 1321N1 GBM cell line since it was comparable to native astrocytes in terms of dopamine, serotonin, norepinephrine, and histamine transport (Naganuma et al., 2014). Thus, the effect of $A_{2A}$AR-bound ANR 672 on spheroids has been studied using 1321N1 GBM cells which overexpresses the A2A receptor. As a preliminary assessment, ANR 672 and ZM241385 were assessed for their ability to induce cell death of 1321N1 grown in 2D environment, in a dose dependent manner. The analysis revealed the $IC_{50}$ values of ANR 672 and ZM241385 to be about 34.1 μM and 164 μM, respectively (Fig. 5**A**). However, the cell death evaluation of the spheroid revealed

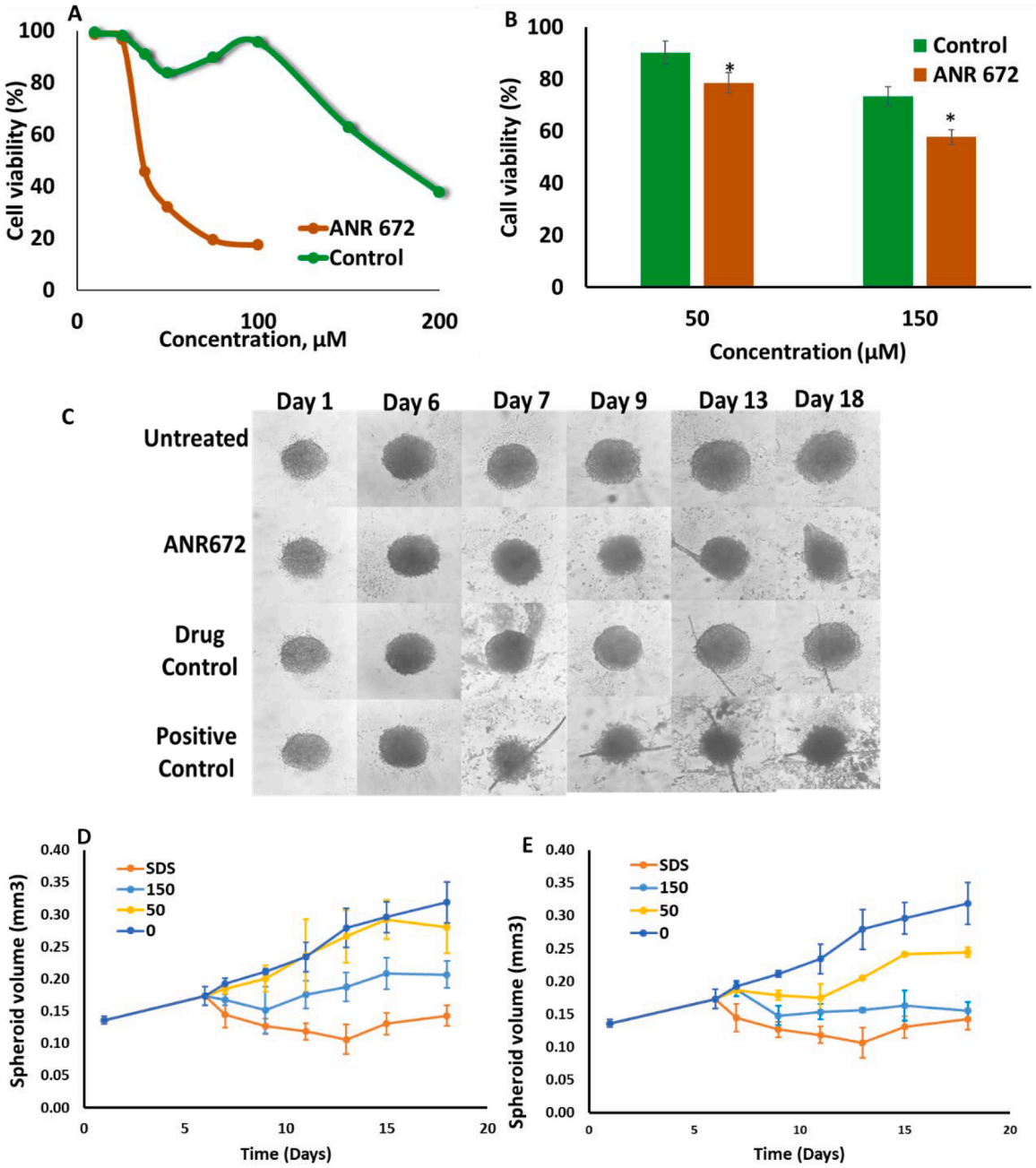


**Fig. 5. Effect of ANR 672 in GBM spheroid growth: (A)** Representative time-lapse image of GBM spheroids obtained from 1321N1 cell, taken over 18 days of treatment with ANR 672, ZM241385 (antagonist drug control), SDS (positive control) and untreated control (Scale bar, 100 µm). Measurement of spheroid volume (mm3) in ZM241385 **(B)** and ANR 672 **(C)** treated 1321N1 cells at the concentration of 50 µM, 150 µM. spheroid volumes were also measured for untreated and SDS controls. **(D)** Spheroid cell viability (%) in control and ANR 672 treated conditions, normalized against untreated. * Represent statistically significant differences between the ANR 672 and control analyzed by Dunnett's test. * $p < 0,05$, ** $p < 0,001$ and ns $p > 0,05$.

that ≈ 90 % and 79 % of GBM cells were viable upon treatment of 50uM concentration of ZM241385 and ANR 672. The addition of higher concentration (150 µM) of ZM241385 and ANR 672 significantly decreased the vitality of spheroid cells, to about 73 % and 58 % cells, respectively (Fig. 5**B**). Tumor spheroids are extensively used to investigate the avascular tumor growth and migration. To study the effect of ANR 672 in a tumor-like environment, three-dimensional (3D) tumor spheroid of GBM cells, 1321N1 were grown. After 6 days of cell culture, images from phase contrast microscopy (Fig. 5**C**) revealed that the 1321N1 cells were developed as a round shape, with a smooth surface and compact morphology. Single spheroids with 90 % specificity were produced using cell-repellent u-shaped bottom plates that had a coefficient of variation (relative standard deviation) of < 5 % in diameter. It was observed that the developed spheroids had an average diameter of 678 µm and eccentricity of 0.37. Fig. 5**C** represents the microscope images of spheroids formed before and after ANR 672 treatment, with ZM241385 as positive control and SDS as drug control, over the period of 18 days. ANR 672 treated spheroids confirmed a considerable reduction in the growth rate than the positive and drug control. There was a significant reduction in the spheroid volume ($mm^3$) over the concentration of ZM241385 and ANR 672 (150 µM < 50 µM < 10 µM). Similar observation was noticed over time with 2.1- and 0.7-fold less in spheroid volume ($mm^3$) in both ANR 672 and ZM241385 treated spheroids respectively (Fig. 5**D and** 5**E**). Therefore, our results suggest that GBM spheroids are more

A

| ADMET | Descriptors | ANR 672 |
|---|---|---|
| Pharmacokinetics | GI absorption | High |
| | BBB permeant | No |
| | Pgp substrate | Yes |
| | CYP1A2 inhibitor | Yes |
| | CYP2C19 inhibitor | Yes |
| | CYP2C9 inhibitor | Yes |
| | CYP2D6 inhibitor | Yes |
| | CYP3A4 inhibitor | Yes |
| | log Kp (cm/s) | -6,47 |
| Druglikeness | Lipinski | 0 |
| | Ghose | 0 |
| | Veber | 0 |
| | Egan | 0 |
| | Muegge | 0 |
| | Bioavailability Score | 0,55 |

B

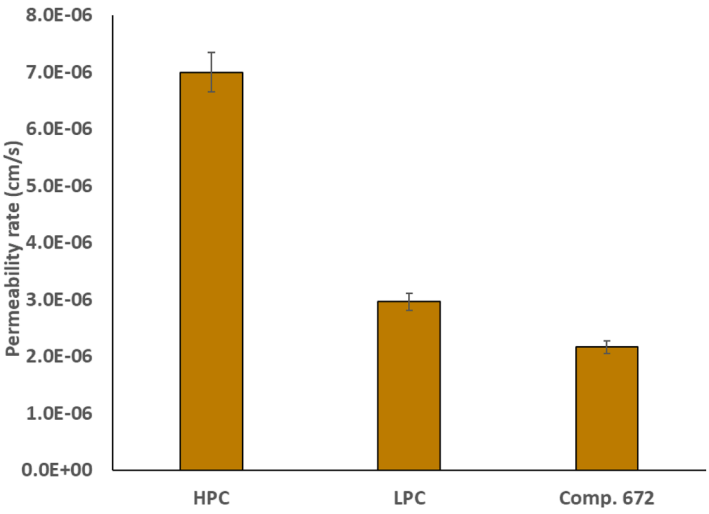


**Fig. 6. ADMET analysis and permeability ability of ANR 672 crossing Blood Brain Barrier (BBB). (A)** SwissADME analysis of the ANR 672 representing the pharmacokinetics and toxicity profile; **(B)** Quantitative measurment of BBB membrane permeability in controls (HPC and LPC) and ANR 672 treated conditions. The error bars denotes the standard deviations from the biolofical repeats n = 5 experiments.

sensitive to ANR 672 than the exiting $A_{2A}$AR antagonist, ZM241385. These results demonstrated that the ANR 672 potentially could inhibit spheroid growth and viability of GBM cells, thereby reducing cancer cell proliferation.

### 3.6. *ANR 672 exhibits drug-like property with BBB crossing potential*

To predict the druglikeness of ANR 672, we performed ADMET analysis using SwissADME that revealed the physicochemical descriptors and pharmacokinetics properties. ANR 672 exhibits satisfactory ADMET characteristics that are represented in the Fig. 6**A**. Several parameters recommended by SwissADME were screened. The HIA adsorption value was found to be higher, ensuring oral absorption potential of the drug. ANR 672 was also found to be an inhibitor of Pgp substrate, CYP1A2, CYP2C19, CYP2C9, CYP2D6 and CYP3A4, which is an important feature when evaluating possible drug interactions. In addition, the bioavailability score of the compound was 0.55 suggesting that ANR 672 could be orally administered, be absorbed by the gastrointestinal tract and reach the systemic circulation. Despite its good distribution and excretion characteristics, our prediction showed that ANR 672 would have relatively no blood-brain barrier (BBB) permeability. Since the ANR 672's bioavailability and its ability to cross BBB is crucial to function as an anti-GBM drug, we further validated using parallel artificial membrane permeation assay (PAMPA). The PAMPA permeability ($P_e$) analysis revealed that when compared to controls (HPC & LPC), ANR 672 had lower BBB crossing potential. Specifically, HPC and LPC BBB showed the $P_e > 4 \times 10^{-6}$ cm/s and $P_e < 4 \times 10^{-6}$ cm/s, respectively whereas ANR 672 has a permeability of $2.1 \times 10^{-6}$ cm/s, which deviates from the in-silico predictions (Fig. 6**B**). These analyses revealed that ANR 672 has good distribution and excretion with the modest BBB crossing potential.

## 4. Discussion

Adenosine plays a crucial role in the progression of tumour and drug resistance. Specifically, the adenosine binding receptor, subtype $A_{2A}$, is primarily implicated in the control of extracellular adenosine in tumour microenvironments. Previous studies on GBM cells, U87MG, U373MG, and ASB19, revealed that pharmacological treatment with the adenosine inhibitor, ATB702 dichloride hydrate (IC = 1.7 nM), increased the level of adenosine in the tumor cells (Jarvis et al., 2000; Marcelino et al., 2021). The increase in adenosine and their interaction with $A_{2A}$ receptor subsequently produce Interleukin-17A (IL-17A), which in turns induce GBM cell migration and invasion through the activation of phosphatidylinositol 3-kinases/protein kinase B (PI3K/AKT) signaling pathway. Overexpression of adenosine also protects GBM cells from the chemotherapeutic drug temozolomide. Preclinical research with the $A_{2A}$AR antagonist, SCH58261, in treating head and neck squamous cell cancer (HNSCC) demonstrated improved outcomes. Similarly, the FDA approved $A_{2A}$ targeting antagonistic drug istradefylline also inhibited the migration, adhesion, and colony formation in melanoma cells. To date, no convincing study has been explored in developing a potential antagonist for blocking the $A_{2A}$AR signaling pathway for the treatment of GBM.

The current study focuses on the functionality of the newly synthesized adenosine derivatives ANR 681, ANR 672, ANR 668, ANR 665, ANR 474, and ANR 94 as potential $A_{2A}$AR antagonists. A pilot investigation on GBM cells, SNB19, revealed ANR 672 possessing stronger antiproliferative effect than the other investigated ANR derivatives. This finding implies that ANR 672 may have more specific and potential interaction features with $A_{2A}$AR and impede its downstream signaling pathway via cAMP inhibition. In line with our previous observations on ANR derivatives interaction with $A_{2A}$AR, the ANR 672 exhibits lowest $K_i$ of $1.02 \pm 0.06$ nM while ANR 665, ANR 668, ANR 681, ANR 474 and ANR 94 showed the $K_i$ of $123 \pm 2$ nM, $76.2 \pm 17.3$ nM, $3478 \pm 312$ nM, $1.82 \pm 0.01$ nM and $45 \pm 13$ nM, respectively (Supplemental Table). This indicates that ANR 672 could have strong binding with $A_{2A}$AR. The pharmacological treatment of these derivative has already proven to activate neuroprotective mechanism, highlighting that ANR 672 functions as a neuroprotective agent, while it decreases the GBM progression. In the present research, we found that addition of ANR 672 increased mouse embryonic fibroblasts' proliferation, while decreased GBM cell growth, indicating that ANR 672 has adopted a different mechanism in normal cells than malignant cells. Previously, it was also found that ADK inhibitors ABT 702 and ITU significantly suppressed the proliferation of GBM cells. In line with our findings, blocking $A_{2A}$AR with ANR 672 may function as an ADK inhibitor, since it regulates the degree of intra and extracellular adenosine transport, which is crucial in GBM prognosis and therapy.

It was identified that adenosine can induce cell death by specific extracellular receptor activation, or it can enter cells directly to exert its toxicity (Abbracchio et al., 1997). The role of $A_{2B}$AR and its related

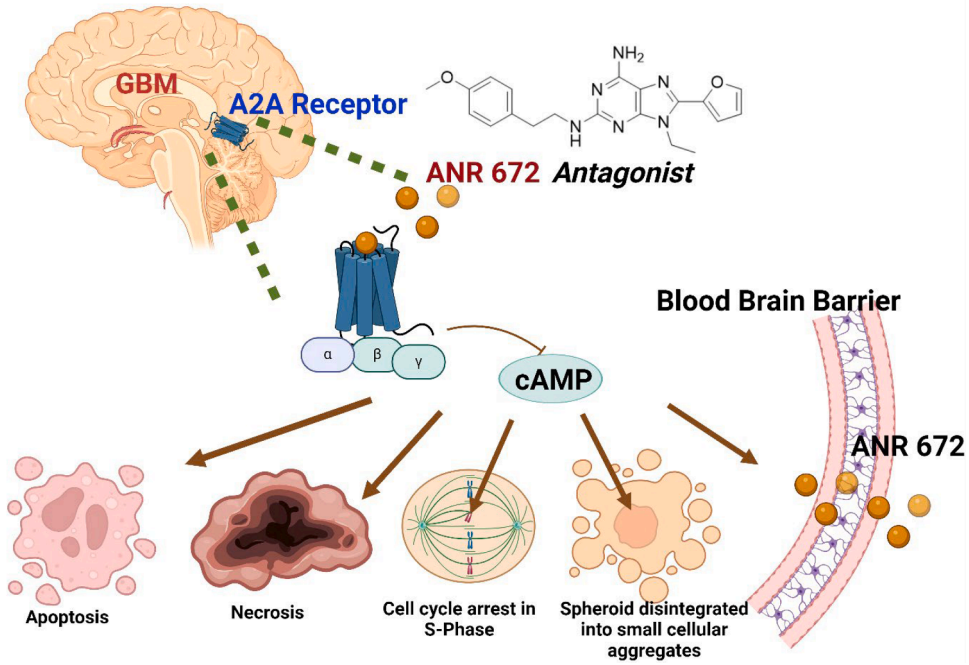


**Fig. 7.** $A_{2A}$ adenosine receptors-triggered signal transduction cascade in GBM cancer cells. ANR 672 antagonist inhibits A2AAR signaling. This process induces apoptosis, necrosis, cell cycle arrest, and spheroid growth arrest, with the ability to penetrate the blood-brain barrier.

signaling pathways has been investigated in a variety of human tumor types (Sun and Huang, 2016), and it has been discovered that $A_{2B}$AR can cause apoptosis in colon and ovarian cancer cells (Hajiahmadi et al., 2015; Long et al., 2013). Mittal et al. (Mittal et al., 2016) showed that $A_{2B}$AR may promote tumor metastasis, and $A_{2B}$AR inhibition has been observed to decrease the growth and metastasis of prostate cancer and melanoma cells (Iannone et al., 2013; Wei et al., 2013). Similarly, our findings revealed the potential function of ANR 672 in triggering necrosis-mediated cell death, which could be attributed to its ability to activate the specific adenosine receptor $A_{2A}$AR in GBM cells, which then triggers a downstream signaling cascade that enhances cell death.

Another significant approach to prevent the tumor growth is through the modulation of the cell cycle progression. We have observed that ANR 672 was able to arrest the cells mostly in S phase than the G1 and G2 phase. Our data has been supported by several report on the regulation of cell cycle at G1/S phase, which is steered by the downregulation of CDK4 and cyclin complex (Aghaei et al., 2012; Shirali et al., 2013). Furthermore, we were able to observe the blockade of $A_{2A}$AR by ANR 672 thereby decreasing the GBM spheroid growth, which further supported the fact that it has the potential to slow down the GBM tumor growth, and thereby leading to prolonged patient longevity. We also identified the use of ANR 672 as a suitable drug target by checking its ability to cross the blood brain barrier, along with other ADMET features, implying its further investigation for its therapeutic applications as an anti-GBM drug (Fig. 7).

## 5. Conclusion

In conclusion, the present study showed that the adenosine derivative ANR 672 triggers the GBM necrosis-mediated cell death. Our data also revealed the ability of ANR 672 to arrest the cell cycle at S phase, reducing the tumor spheroid volume, and exhibiting the ability to cross the BBB in a moderate level with the good bioavailability. Although all our findings provide significant *in silico* and *in vitro* experimental evidence, additional phase I clinical trials may support the usage of ANR 672 as an anti-GBM medication.

## CRediT authorship contribution statement

**Akshaya Murugesan:** Writing – review & editing, Writing – original draft, Visualization, Validation, Methodology, Formal analysis. **Aleksei Smirnov:** Writing – original draft, Visualization, Validation, Methodology, Formal analysis. **Anxo Vila Alonso:** Writing – original draft, Visualization, Validation, Methodology, Formal analysis. **Michela Buccioni:** Writing – original draft, Visualization, Validation, Supervision, Resources, Methodology, Investigation. **Chang Cui:** Writing – original draft, Visualization, Methodology, Formal analysis. **Diego Dal Ben:** Writing – original draft, Visualization, Software, Methodology, Formal analysis. **Beatrice Francucci:** Writing – original draft, Visualization, Validation, Methodology, Formal analysis. **Catia Lambertucci:** Writing – original draft, Visualization, Validation, Supervision, Methodology, Formal analysis. **Gabriella Marucci:** Writing – original draft, Validation, Supervision, Resources, Project administration, Funding acquisition, Formal analysis. **Rosaria Volpini:** Writing – original draft, Validation, Supervision, Resources, Investigation, Funding acquisition, Formal analysis. **Saravanan Konda Mani:** Writing – original draft, Visualization, Software, Methodology, Formal analysis. **Sandhanasamy Devanesan:** Writing – original draft, Visualization, Software, Resources. **Mohamad S. AlSalhi:** Writing – original draft, Visualization, Validation, Software, Resources. **Olli Yli-Harja:** Writing – original draft, Visualization, Project administration, Funding acquisition. **Andrea Spinaci:** Writing – review & editing, Writing – original draft, Project administration, Methodology, Funding acquisition, Conceptualization. **Meenakshisundaram Kandhavelu:** Writing – review & editing, Writing – original draft, Visualization, Supervision, Resources, Project administration, Investigation, Funding acquisition, Conceptualization.

## Declaration of competing interest

The authors declare no conflict of interest.

## Acknowledgement

This research was funded by Fondo di Ateneo-per la Ricerca Scientifica (University of Camerino), Grant number FPI002003 and Regione Marche, Project 'Tumori Solidi', Grant number FPI532001. The authors express their sincere appreciation to the Researchers Supporting Project Number (RSP2025R398) King Saud University, Riyadh, Saudi Arabia.

## Supplementary materials

Supplementary material associated with this article can be found, in the online version, at doi:10.1016/j.ejps.2025.107039.

## Data availability

Data will be made available on request.

## References

Abbracchio, M.P., Ceruti, S., Brambilla, R., Franceschi, C., Malorni, W., Jacobson, K.A., von Lubitz, D.K.J.E., Cattabeni, F., 1997. Modulation of apoptosis by adenosine in the central nervous system: a possible role for the a3 receptor. Ann. N. Y. Acad. Sci. 825, 11–22.

Aghaei, M., Karami-Tehrani, F., Panjehpour, M., Salami, S., Fallahian, F., 2012. Adenosine induces cell-cycle arrest and apoptosis in androgen-dependent and -independent prostate cancer cell lines, LNcap-FGC-10, DU-145, and PC3. Prostate 72, 361–375. https://doi.org/10.1002/pros.21438.

Barth, E., Kuczera, K., Leimkuhler, B., Skeel, R.D., 1995. Algorithms for constrained molecular dynamics. J. Comput. Chem. 16, 1192–1209. https://doi.org/10.1002/jcc.540161003.

Bova, V., Filippone, A., Casili, G., Lanza, M., Campolo, M., Capra, A.P., Repici, A., Crupi, L., Motta, G., Colarossi, C., Chisari, G., Cuzzocrea, S., Esposito, E., Paterniti, I., 2022. Adenosine targeting as a new strategy to decrease glioblastoma aggressiveness. Cancers (Basel) 14, 4032. https://doi.org/10.3390/cancers14164032.

Camaioni, E., Costanzi, S., Vittori, S., Volpini, R., Klotz, K.N., Cristalli, G., 1998. New substituted 9-alkylpurines as adenosine receptor ligands. Bioorg. Med. Chem. 6, 523–533. https://doi.org/10.1016/s0968-0896(98)00007-8.

Case, D.A., Cheatham III, T.E., Darden, T., Gohlke, H., Luo, R., Merz Jr., K.M., Onufriev, A., Simmerling, C., Wang, B., Woods, R.J., 2005. The Amber biomolecular simulation programs. J. Comput. Chem. 26, 1668–1688. https://doi.org/10.1002/jcc.20290.

Chen, W., Wong, C., Vosburgh, E., Levine, A.J., Foran, D.J., Xu, E.Y., 2014. High-throughput image analysis of tumor spheroids: a user-friendly software application to measure the size of spheroids automatically and accurately. J. Vis. Exp. 8 (89), 51639. https://doi.org/10.3791/51639.

Chowdhury, S., Kandhavelu, M., Yli-Harja, O., Ribeiro, A.s., 2012. An interacting multiple model filter-based autofocus strategy for confocal time-lapse microscopy. J. Microsc. 245, 265–275. https://doi.org/10.1111/j.1365-2818.2011.03568.x.

Darden, T., York, D., Pedersen, L., 1993. Particle mesh Ewald: An N·log(N) method for Ewald sums in large systems. J. Chem. Phys. 98, 10089–10092. https://doi.org/10.1063/1.464397.

Domènech, M., Hernández, A., Plaja, A., Martínez-Balibrea, E., Balañà, C., 2021. Hypoxia: the cornerstone of glioblastoma. Int. J. Mol. Sci. 22, 12608. https://doi.org/10.3390/ijms222212608.

Doré, A.S., Robertson, N., Errey, J.C., Ng, I., Hollenstein, K., Tehan, B., Hurrell, E., Bennett, K., Congreve, M., Magnani, F., Tate, C.G., Weir, M., Marshall, F.H., 2011. Structure of the adenosine A2A receptor in complex with ZM241385 and the xanthines XAC and caffeine. Structure 19, 1283–1293. https://doi.org/10.1016/j.str.2011.06.014.

Eberhardt, J., Santos-Martins, D., Tillack, A.F., Forli, S., 2021. AutoDock Vina 1.2.0: new docking methods, expanded force field, and python bindings. J. Chem. Inf. Model. 61, 3891–3898. https://doi.org/10.1021/acs.jcim.1c00203.

Erices, J.I., Bizama, C., Niechi, I., Uribe, D., Rosales, A., Fabres, K., Navarro-Martínez, G., Torres, Á., San Martín, R., Roa, J.C., Quezada-Monrás, C., 2023. Glioblastoma microenvironment and invasiveness: new insights and therapeutic targets. Int. J. Mol. Sci. 24, 7047. https://doi.org/10.3390/ijms24087047.

Hajiahmadi, S., Panjehpour, M., Aghaei, M., Shabani, M., 2015. Activation of A2b adenosine receptor regulates ovarian cancer cell growth: involvement of Bax/Bcl-2 and caspase-3. Biochem. Cell Biol. 93, 321–329. https://doi.org/10.1139/bcb-2014-0117.

Iannone, R., Miele, L., Maiolino, P., Pinto, A., Morello, S., 2013. Blockade of A2b adenosine receptor reduces tumor growth and immune suppression mediated by myeloid-derived suppressor cells in a mouse model of melanoma. Neoplasia 15, 1400–1409. https://doi.org/10.1593/neo.131748.

Izadi, S., Anandakrishnan, R., Onufriev, A.V., 2014. Building Water Models: A Different Approach. J. Phys. Chem. Lett. 5, 3863–3871. https://doi.org/10.1021/jz501780a.

Jackson, S., Anders, N.M., Mangraviti, A., Wanjiku, T.M., Sankey, E.W., Liu, A., Brem, H., Tyler, B., Rudek, M.A., Grossman, S.A., 2016. The effect of regadenoson-induced transient disruption of the blood–brain barrier on temozolomide delivery to normal rat brain. J. Neurooncol. 126, 433–439. https://doi.org/10.1007/s11060-015-1998-4.

Jarvis, M.F., Yu, H., Kohlhaas, K., Alexander, K., Lee, C.-H., Jiang, M., Bhagwat, S.S., Williams, M., Kowaluk, E.A., 2000. ABT-702 (4-Amino-5-(3-bromophenyl)-7-(6-morpholinopyridin-3-yl)pyrido[2,3-d]pyrimidine), a Novel Orally Effective Adenosine Kinase Inhibitor with Analgesic and Anti-Inflammatory Properties: I. In Vitro Characterization and Acute Antinociceptive Effects in the Mouse. J. Pharmacol. Exp. Ther. 295, 1156–1164.

Jin, K., Mao, C., Chen, L., Wang, L., Liu, Y., Yuan, J., 2021. Adenosinergic Pathway: A Hope in the Immunotherapy of Glioblastoma. Cancers (Basel) 13, 229. https://doi.org/10.3390/cancers13020229.

Kari, S., Subramanian, K., Altomonte, I.A., Murugesan, A., Yli-Harja, O., Kandhavelu, M., 2022. Programmed cell death detection methods: a systematic review and a categorical comparison. Apoptosis 27, 482–508. https://doi.org/10.1007/s10495-022-01735-y.

Karjalainen, A., Doan, P., Chandraseelan, J.G., Sandberg, O., Yli-Harja, O., Candeias, N. R., Kandhavelu, M., 2017. Synthesis of phenol-derivatives and biological screening for anticancer activity. Anti-Cancer Agents Med. Chemi. (Formerly Curr. Med. Chem.-Anti-Cancer Agents) 17, 1710–1720.

Klowss, J.J., Browning, A.P., Murphy, R.J., Carr, E.J., Plank, M.J., Gunasingh, G., Haass, N.K., Simpson, M.J., n.d. A stochastic mathematical model of 4D tumour spheroids with real-time fluorescent cell cycle labelling. J. R. Soc. Interface 19, 20210903. https://doi.org/10.1098/rsif.2021.0903.

Krog, D., Enghoff, M.B., Köhn, C., 2023. A Monte Carlo approach to study the effect of ions on the nucleation of sulfuric acid–water clusters. J. Comput. Chem. 44, 1250–1262. https://doi.org/10.1002/jcc.27076.

Leone, R.D., Emens, L.A., 2018. Targeting adenosine for cancer immunotherapy. J. ImmunOther. Cancer 6, 57. https://doi.org/10.1186/s40425-018-0360-8.

Liew, K.F., Chan, K.L., Lee, C.Y., 2015. Blood-brain barrier permeable anticholinesterase aurones: synthesis, structure-activity relationship, and drug-like properties. Eur. J. Med. Chem. 94, 195–210. https://doi.org/10.1016/j.ejmech.2015.02.055.

Long, J.S., Crighton, D., O'Prey, J., Mackay, G., Zheng, L., Palmer, T.M., Gottlieb, E., Ryan, K.M., 2013. Extracellular adenosine sensing-a metabolic cell death priming mechanism downstream of p53. Mol. Cell 50, 394–406. https://doi.org/10.1016/j.molcel.2013.03.016.

Ma, X.-L., Shen, M.-N., Hu, B., Wang, B.-L., Yang, W.-J., Lv, L.-H., Wang, H., Zhou, Y., Jin, A.-L., Sun, Y.-F., Zhang, C.-Y., Qiu, S.-J., Pan, B.-S., Zhou, J., Fan, J., Yang, X.-R., Guo, W., 2019. CD73 promotes hepatocellular carcinoma progression and metastasis via activating PI3K/AKT signaling by inducing Rap1-mediated membrane localization of P110β and predicts poor prognosis. J. Hematol. Oncol. 12, 37. https://doi.org/10.1186/s13045-019-0724-7.

Marcelino, H., Carvalho, T.M.A., Tomás, J., Teles, F.I., Honório, A.C., Rosa, C.B., Costa, A.R., Costa, B.M., Santos, C.R.A., Sebastião, A.M., Cascalheira, J.F., 2021. Adenosine inhibits cell proliferation differently in human astrocytes and in glioblastoma cell lines. Neuroscience 467, 122–133. https://doi.org/10.1016/j.neuroscience.2021.05.019.

Marucci, G., Finaurini, S., Buccioni, M., Lammi, C., Kandhavelu, M., Volpini, R., Ricciutelli, M., Angeli, P., Commandeur, J.N.M., Cristalli, G., 2008. In Vitro metabolism studies of new adenosine a. Drug Metab. Lett. 2, 301–307. https://doi.org/10.2174/187231208786734076.

Marucci, G., Santinelli, C., Buccioni, M., Navia, A.M., Lambertucci, C., Zhurina, A., Yli-Harja, O., Volpini, R., Kandhavelu, M., 2018. Anticancer activity study of A3 adenosine receptor agonists. Life Sci. 205, 155–163. https://doi.org/10.1016/j.lfs.2018.05.028.

Mittal, D., Sinha, D., Barkauskas, D., Young, A., Kalimutho, M., Stannard, K., Caramia, F., Haibe-Kains, B., Stagg, J., Khanna, K.K., Loi, S., Smyth, M.J., 2016. Adenosine 2B receptor expression on cancer cells promotes metastasis. Cancer Res. 76, 4372–4382. https://doi.org/10.1158/0008-5472.CAN-16-0544.

Mohan, A.A., Tomaszewski, W.H., Haskell-Mendoza, A.P., Hotchkiss, K.M., Singh, K., Reedy, J.L., Fecci, P.E., Sampson, J.H., Khasraw, M., 2021. Targeting Immunometabolism in Glioblastoma. Front. Oncol. 11, 696402. https://doi.org/10.3389/fonc.2021.696402.

Mutharasu, G., Murugesan, A., Konda Mani, S., Yli-Harja, O., Kandhavelu, M., 2022. Transcriptomic analysis of glioblastoma multiforme providing new insights into GPR17 signaling communication. J. Biomol. Struct. Dyn. 40, 2586–2599. https://doi.org/10.1080/07391102.2020.1841029.

Naganuma, F., Yoshikawa, T., Nakamura, T., Iida, T., Harada, R., Mohsen, A.S., Miura, Y., Yanai, K., 2014. Predominant role of plasma membrane monoamine transporters in monoamine transport in 1321N1, a human astrocytoma-derived cell line. J. Neurochem. 129, 591–601. https://doi.org/10.1111/jnc.12665.

Pinna, A., Volpini, R., Cristalli, G., Morelli, M., 2005. New adenosine A2A receptor antagonists: actions on Parkinson's disease models. Eur. J. Pharmacol. 512, 157–164. https://doi.org/10.1016/j.ejphar.2005.01.057.

Shirali, S., Aghaei, M., Shabani, M., Fathi, M., Sohrabi, M., Moeinifard, M., 2013. Adenosine induces cell cycle arrest and apoptosis via cyclinD1/Cdk4 and Bcl-2/Bax pathways in human ovarian cancer cell line OVCAR-3. Tumour. Biol. 34, 1085–1095. https://doi.org/10.1007/s13277-013-0650-1.

Sidders, B., Zhang, P., Goodwin, K., O'Connor, G., Russell, D.L., Borodovsky, A., Armenia, J., McEwen, R., Linghu, B., Bendell, J.C., Bauer, T.M., Patel, M.R., Falchook, G.S., Merchant, M., Pouliot, G., Barrett, J.C., Dry, J.R., Woessner, R., Sachsenmeier, K., 2020. Adenosine signaling is prognostic for cancer outcome and

has predictive utility for immunotherapeutic response. Clin. Cancer Res. 26, 2176–2187. https://doi.org/10.1158/1078-0432.CCR-19-2183.

Spinaci, A., Buccioni, M., Catarzi, D., Cui, C., Colotta, V., Dal Ben, D., Cescon, E., Francucci, B., Grieco, I., Lambertucci, C., Marucci, G., Bassani, D., Pavan, M., Varano, F., Federico, S., Spalluto, G., Moro, S., Volpini, R., 2023. Dual anta-inhibitors" of the A2A adenosine receptor and casein kinase ck1delta: synthesis, biological evaluation, and molecular modeling studies. Pharmaceuticals (Basel) 16, 167. https://doi.org/10.3390/ph16020167.

Spinaci, A., Lambertucci, C., Buccioni, M., Dal Ben, D., Graiff, C., Barbalace, M.C., Hrelia, S., Angeloni, C., Tayebati, S.K., Ubaldi, M., Masi, A., Klotz, K.-N., Volpini, R., Marucci, G., 2022. A2A adenosine receptor antagonists: are triazolotriazine and purine scaffolds interchangeable? Molecules. 27, 2386. https://doi.org/10.3390/molecules27082386.

Sun, Y., Huang, P., 2016. Adenosine A2B receptor: from cell biology to human diseases. Front. Chem. 4, 37. https://doi.org/10.3389/fchem.2016.00037.

Tamimi, A.F., Juweid, M., 2017. Epidemiology and Outcome of Glioblastoma, in: De Vleeschouwer, S. (Ed.), Glioblastoma. Codon Publications, Brisbane (AU).

Wei, Q., Costanzi, S., Balasubramanian, R., Gao, Z.-G., Jacobson, K.A., 2013. A2B adenosine receptor blockade inhibits growth of prostate cancer cells. Purinergic. Signal. 9, 271–280. https://doi.org/10.1007/s11302-012-9350-3.

Wishart, D.S., Knox, C., Guo, A.C., Shrivastava, S., Hassanali, M., Stothard, P., Chang, Z., Woolsey, J., 2006. DrugBank: a comprehensive resource for in silico drug discovery and exploration. Nucleic. Acids. Res. 34, D668–D672. https://doi.org/10.1093/nar/gkj067.

Xia, C., Yin, S., To, K.K.W., Fu, L., 2023. CD39/CD73/A2AR pathway and cancer immunotherapy. Mol. Cancer 22, 44. https://doi.org/10.1186/s12943-023-01733-x.